ARCHIVES OF ELECTRICAL ENGINEERING VOL. 70(1), pp. 37–51 (2021)

DOI 10.24425/aee.2021.136051

Experimental study on fault ride-through capability of VSC-based HVDC transmission system

NGO MINH KHOA, NGUYEN AN TOAN, DOAN DUC TUNG

Faculty of Engineering and Technology, Quynhon University
Vietnam

e-mails: {ngominhkhoa/nguyenantoan/doanductung}@qnu.edu.vn

(Received: 13.04.2020, revised: 18.08.2020)

Abstract: For voltage-source-converter based high-voltage-direct-current (VSC-HVDC) transmission systems, fault ride-through (FRT) capability is a very important grid requirement in order to enhance its operational availability under an alternating current (AC) grid fault condition. Voltage sags during a short-circuit fault in power transmission lines can lead to fluctuations in the direct current (DC) link voltage of converter systems, and may induce reversed power flow and even trip a VSC-HVDC transmission system. A practical method is developed in this paper for investigating FRT capability of VSC-HVDC transmission system characteristics during a voltage sag event using experimental results from Smart Grid Laboratory. Symmetrical and asymmetrical voltage sag events with different remaining voltages are applied to an AC grid that lasts with a variable duration. The experimental waveforms of the two converter systems are recorded and analyzed in order to evaluate the FRT capability of VSC-HVDC transmission systems.

Key words: converter system, experimental waveform, fault ride-through, high-voltage direct current, voltage sag

1. Introduction

The development of national and international interconnected networks has necessitated a bridging of relatively long distances in some cases. In the case of 3-phase alternating current (AC) power, this has given rise to stability problems attributable to the different voltage angles between a line's beginning and ending [1–3]. Furthermore, a line produces or consumes reactive power depending on whether the load on the line is low or high. Due to their high mutual capacitance, cable routes without elaborate compensation facilities can be established

only up to the length of a transmission line. Efforts were, therefore, made at an early stage to also use high direct current (DC) voltages for power transmission [4, 5]. One challenge for voltage-source-converter based high-voltage-direct-current (VSC-HVDC) transmission systems is the fault ride-through (FRT) capability which is specified by grid codes [4–6]. The FRT capability allows VSC-HVDC transmission systems to remain a normally operating status during abnormal AC grid conditions like voltage deviations [7, 8]. The FRT requirement consists of zero voltage ride-through (ZVRT), low voltage ride-through (LVRT), and high-voltage ride-through (HVRT).

The FRT has attracted widespread scientific attention, most of them are mainly studying methods for enhancing the FRT capability of wind turbines connected to an AC grid through a VSC-HVDC transmission system [9–16]. The authors in [9] proposed a new control approach for securing fault ride-through of wind. The approach in [10] could improve the FRT capability of wind farms by using a nonlinear adaptive control of VSC-HVDC. The control method could block the converters for a short-time and could take corresponding actions to diminish the post-fault disturbances. The over-current was limited, the wind turbines managed to remain connected, and the AC voltage recovered quickly [11]. The work in [12] presented an FRT protection method for a wind farm connected to an AC grid through an HVDC link. In [13], an FRT strategy for offshore wind farms connected to the grid through a VSC-HVDC transmission system was proposed to introduce a controlled voltage drop at the offshore grid when a fault occurred at the onshore side. The DC fault recovery strategy proposed in [14] applied a high rating series diode valve located at each VSC inverter pole for reducing fault currents. The schemes of the FRT control and management for the VSC-HVDC system were proposed in [15, 16].

The control strategy of converters in VSC-HVDC plays an important role for enhancing its FRT capability [17–22]. In [17], a strategy for reducing the inverter-side overvoltage of the HVDC system under a fault in the inverter-side AC system was proposed. The authors in [18] presented a new static synchronous compensator model of operation for the recently published alternate arm converter. The new FRT method proposed in [19] was without any direct information exchange between two Double-Star Chopper-Cell (DSCC) converters. The authors in [20] developed a perturbation observer-based sliding-mode scheme in order to control VSC-HVDC systems. The scheme did not require an accurate system model and only one state measurement was needed to estimate online the nonlinearities, parameter uncertainties, unmodelled dynamics and time-varying external disturbances of VSC-HVDC systems. For multi-terminal VSC-HVDC systems, the passive control scheme was proposed in [21] to provide a reliable and effective integration of electrical power from renewable energy. The negative sequence controller, which is required for such asymmetrical conditions in AC grids, was proposed by the authors in [22].

This paper aims to study the FRT capability of VSC-HVDC systems under symmetrical and asymmetrical voltage sag events. A practical method is developed in this work by using practical modules of the VSC-HVDC transmission system in our laboratory in order to carry case studies. All experimental results are carefully analyzed for the purpose of evaluating the FRT capability of the VSC-HVDC system. The main contributions presented in this paper are as follows:

(*i*) To develop a practical method for testing the FRT capability of VSC-HVDC systems based on the platform in a laboratory environment.

(*ii*) To give an extensive experimental verification of the proportional integral (PI) control performance of VSCs under different voltage sag types.

2. Background and methodology

2.1. VSC-HVDC Configuration and modelling

The studied system in a laboratory environment is illustrated in Fig. 1, wherein an HVDC system is used to connect two AC grids. The two converter systems can be considered as the composition of two constant-frequency VSC systems: the left-hand-side VSC system is a DC-link voltage controller and the right-hand-side VSC system is an active/reactive power controller. As shown in Fig. 1, the DC-link voltage controller and the active/reactive power controller are interfaced with Grid 1 and Grid 2, respectively. The DC-link voltage controller and the active/reactive power controller are connected in parallel from their DC-side terminals. The left-hand side VSC system, that is, the DC-link voltage controller, provides the DC voltage support to the active/reactive power controller. The active/reactive power controller can independently control the active and reactive power exchanged with Grid 2, that is, P_{s2} and Q_{s2} [23, 24].

The global mathematical model of the overall VSC-HVDC system is expressed as follows:

$$\begin{cases} \dfrac{\mathrm{d}i_{d1}}{\mathrm{d}t} = -\dfrac{R_1}{L_1}i_{d1} + \omega i_{q1} + \dfrac{V_{sd1} - V_{cd1}}{L_1} \\ \dfrac{\mathrm{d}i_{q1}}{\mathrm{d}t} = -\dfrac{R_1}{L_1}i_{q1} - \omega i_{d1} - \dfrac{V_{cq1}}{L_1} \\ \dfrac{\mathrm{d}i_{d2}}{\mathrm{d}t} = -\dfrac{R_2}{L_2}i_{d2} + \omega i_{q2} + \dfrac{V_{sd2} - V_{cd2}}{L_2} \\ \dfrac{\mathrm{d}i_{q2}}{\mathrm{d}t} = -\dfrac{R_2}{L_2}i_{q2} - \omega i_{d2} - \dfrac{V_{cq2}}{L_2} \\ \dfrac{\mathrm{d}V_{DC1}}{\mathrm{d}t} = \dfrac{3V_{sq1}i_{q1}}{2C_{DC1}V_{DC1}} - \dfrac{I_{DC}}{C_{DC1}} \\ \dfrac{\mathrm{d}V_{DC2}}{\mathrm{d}t} = \dfrac{3V_{sq2}i_{q2}}{2C_{DC2}V_{DC2}} - \dfrac{I_{DC}}{C_{DC2}} \\ \dfrac{\mathrm{d}I_{DC}}{\mathrm{d}t} = \dfrac{1}{L_{DC}}(V_{DC1} - V_{DC2}) - \dfrac{R_{DC}}{L_{DC}}I_{DC} \end{cases} . \tag{1}$$

The active and reactive powers entering both VSC1 and VSC2 can be expressed as:

$$\begin{cases} P_1 = \dfrac{3}{2}\left(V_{sq1}i_{q1} + V_{sd1}i_{d1}\right) = \dfrac{3}{2}\left(V_{sq1}i_{q1}\right) \\ Q_1 = \dfrac{3}{2}\left(V_{sq1}i_{d1} + V_{sd1}i_{q1}\right) = \dfrac{3}{2}\left(V_{sq1}i_{d1}\right) \\ P_2 = \dfrac{3}{2}\left(V_{sq2}i_{q2} + V_{sd2}i_{d2}\right) = \dfrac{3}{2}\left(V_{sq2}i_{q2}\right) \\ Q_2 = \dfrac{3}{2}\left(V_{sq2}i_{d2} + V_{sd2}i_{d2}\right) = \dfrac{3}{2}\left(V_{sq2}i_{d2}\right) \end{cases} , \tag{2}$$

where number 1, 2 subscripts denote the variable corresponding to VSC1 and VSC2.

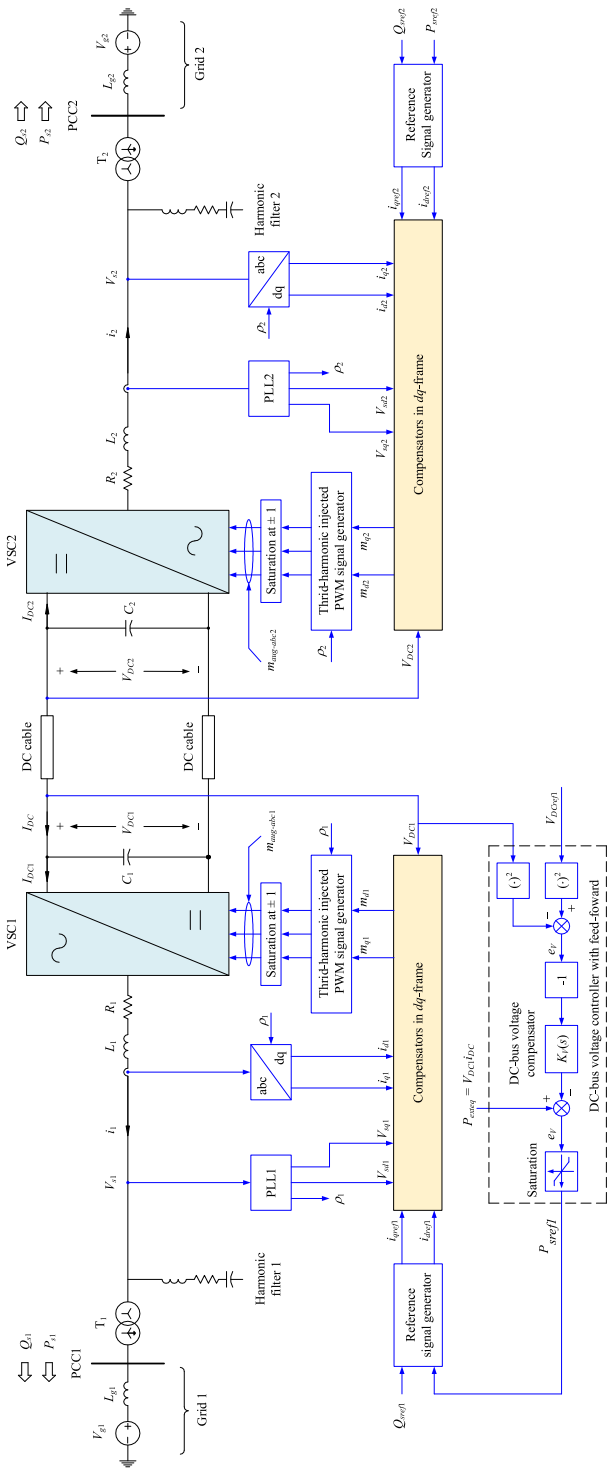

Fig. 1. Configuration of VSC-HVDC transmission system

2.2. Development of practical method

An experimental setup applied to emulate the VSC-HVDC transmission system of Smart Grid Laboratory at our university is shown in Fig. 2(a). Main elements include converter system 1 (VSC1), converter system 2 (VSC2), a DC cable, a dynamic grid fault simulator, an adjustable 3-phase power supply (Grid 1) and a 3-phase power supply (Grid 2). The nominal frequency and voltage of two AC grids in this system are 50 Hz and 380 V, respectively. The VSC-HVDC system parameters are given in Table 1. Besides, both VSC1 and VSC2 can control active power in the DC cable in both directions, can be coupled to the power grid at various frequencies, and can automatically control active/reactive power, and voltage. The conventional PI controllers are applied to VSC-HVDC systems. The PI control parameters can be optimally chosen and tuned by a meta-heuristic algorithm to obtain the optimal control performance [25]. In this paper, the conventional PI controllers, control parameters of which are presented in Table 2, are also applied to VSC-HVDC systems.

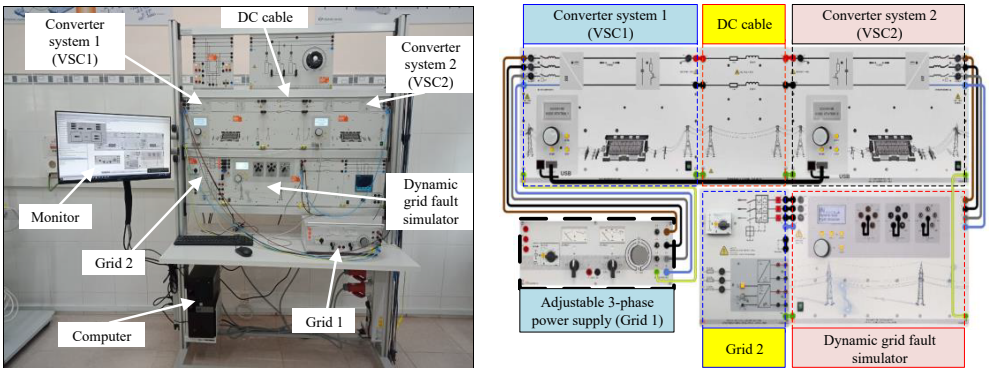

(a) Experimental setup (b) Wiring diagram

Fig. 2. The laboratory prototype for testing the FRT capability of VSC-HVDC transmission system

The VSC-HVDC system is installed for education purposes at the authors' univeristy, it can only transmit up to 1 kW of active power, provide up to 1 kvar of reactive power, and has adjustable DC-link voltage up to 700 VDC. Besides, converter system 1 (VSC1) and converter system 2 (VSC2) are also communicated with a personal computer (PC) which installed an Interactive Lab Assistant course for setting, monitoring, and recording all experimental results. The DC cable in this VSC-HVDC system is to model a 300 km HVDC transmission line. Its resistance and inductance per phase are 7.2 Ohm and 230 mH, respectively. The DC cable can carry a maximum current of 2 A, 700 VDC. In order to establish a fault in an AC grid, the dynamic grid fault simulator in the VSC-HVDC system can perform the function. This module can be used to set up symmetrical and asymmetrical voltage sags in an AC grid with an adjustable remaining voltage for three phases and adjustable duration of the fault from 50 ms to 1000 ms. In addition, the jump angle of voltage sag events which is generated by this module can be varied for analyzing the FRT capability of the VSC-HVDC system. The experiments described in this paper were carried out according to the experimental setup, the wiring diagram of which is shown in Fig. 2(b).

Table 1. The VSC-HVDC system parameters

Adjustable 3-phase power supply (Grid 1)	
Maximum voltage V_{s1} [V]	400
Nominal frequency f_{s1} [Hz]	50
Grid 2	
Nominal voltageV_{s2} [V]	380
Nominal frequencyf_{s2} [Hz]	50
DC cable	
Base DC voltage V_{DCbase} [V]	700
DC resistanceR_{DC} [Ω]	7.2
DC inductance L_{DC} [mH]	230

Table 2. The PI controller parameters of VSCs

Converter system 1 (VSC1)	
Inductance L_1 [μF]	83
Resistance R_1 [mΩ]	1.3
DC bus capacitance C_1 [μF]	73.33
Closed-loop time constant τ_{i1} [ms]	1
Proportional gain k_{p1}	0.083
Integral gain k_{i1}	1.3
Converter system 2 (VSC2)	
Inductance L_2 [μF]	83
Resistance R_2 [mΩ]	1.3
DC bus capacitance C_2 [μF]	73.33
Closed-loop time constant τ_{i2} [ms]	1
Proportional gain k_{p2}	0.083
Integral gain k_{i2}	1.3

A practical method shown in Fig. 3 is developed in this paper to study the FRT capability of VSC-HVDC systems. Using the dynamic fault simulator to create types of voltage sags at the AC grids, the FRT experiments are carried out on the experimental setup. The status of converter systems can be used to evaluate the FRT capability of VSC-HVDC systems. Moreover, all recorded data of these experiments is used to analyze offline and the FRT requirement of the VSC-HVDC system is applied to compare with the experimental results.

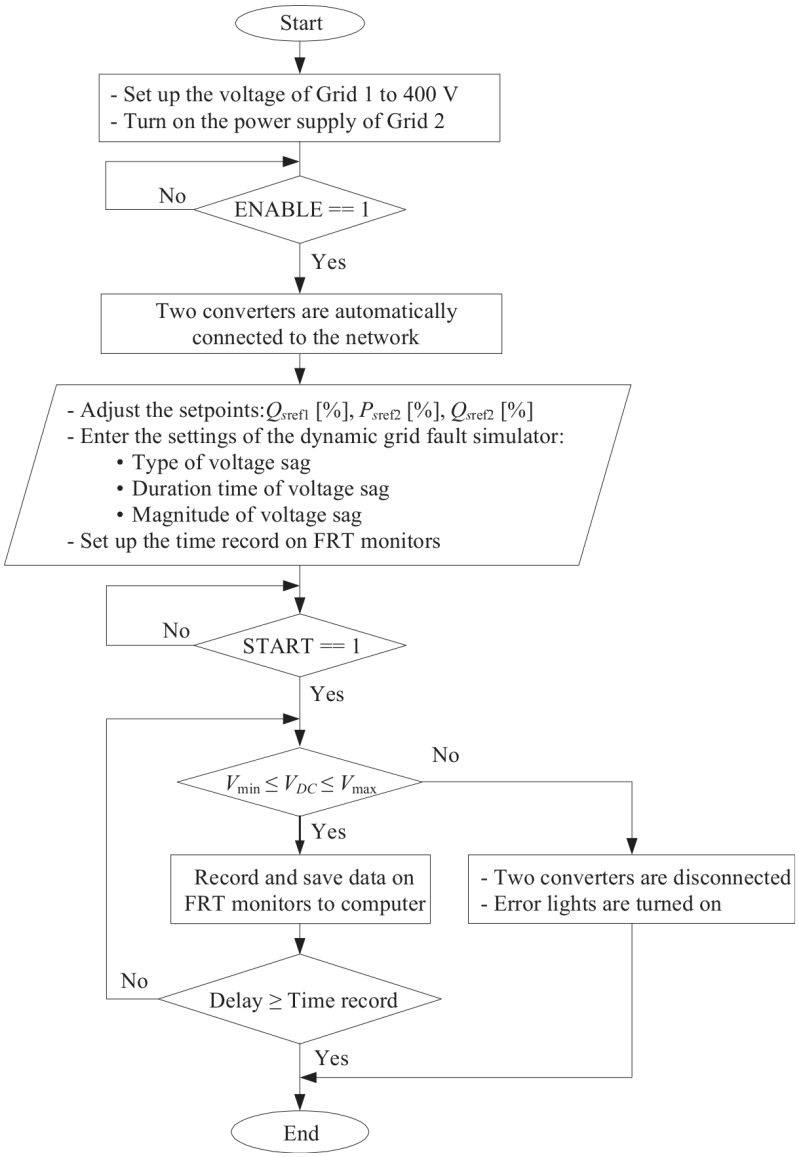

Fig. 3. The flowchart of the practical method for testing the FRT capability of VSC-HVDC system

3. Experimental results and discussion

In order to study the effectiveness of the FRT capability of the VSC-HVDC transmission system shown in Fig. 1 in the case of symmetrical and asymmetrical voltage sag events, three case studies have been carried out and described in this paper. The first case study considers a three-phase voltage sag at the point of common coupling PCC2 (or Grid 2). The second case

study examines the recovery strategy when the VSC-HVDC system is subjected to a two-phase voltage sag at the point of common coupling PCC2. Finally, the third case study considers a single-phase voltage sag at the point of common coupling PCC2. The voltage sag of the three case studies that occurred in Grid 2 has a depth of 60% and a duration time of 200 ms. The following will investigate three case studies in order to analyse and evaluate the FRT capability of the VSC-HVDC transmission system.

Case 1: Three-phase voltage sag

In this case, using a dynamic grid fault simulator, we establish a three-phase voltage sag at the point of common coupling PCC2 (Grid 2), with a depth of 60% and a time duration of 200 ms. In a steady state before the voltage sag is started, the converter system, VSC2, is set to an active/reactive power setting of P_{sref2} = 80% or P_{sref2} = 800 W, Q_{sref2} = 0% or Q_{sref2} = 0 kVAR and the active power is transmitted in the DC cable by the direction from Grid 1 to Grid 2. In this stage, the VSC-HVDC system is normally operated; therefore, three-phase AC voltages and currents are balanced and constant, as shown in the period from 0 ms to 100 ms. Fig. 4(a) and Fig. 4(b) show experimental waveforms of Case 1 which are recorded at VSC1 and VSC2, respectively. In each figure, the first and second plots represent the three-phase voltage and current waveforms at the AC grid to which the VSC is connected, the third and fourth plots show the DC voltage and the DC power at the DC-link circuit of the VSC. Because the three-phase voltage sag in this case occurs at the point of common coupling PCC2 (Grid 2), the magnitude of three-phase voltages at VSC2 is evenly decreased to 0.4 pu (or 92 V) in a short time of the voltage sag (from 100 ms to 300 ms), as shown in the first plot of Fig. 4(b). Before, while and after three-phase voltage sag occurs at Grid 2, the magnitude of three-phase voltages at VSC1 is not still varied

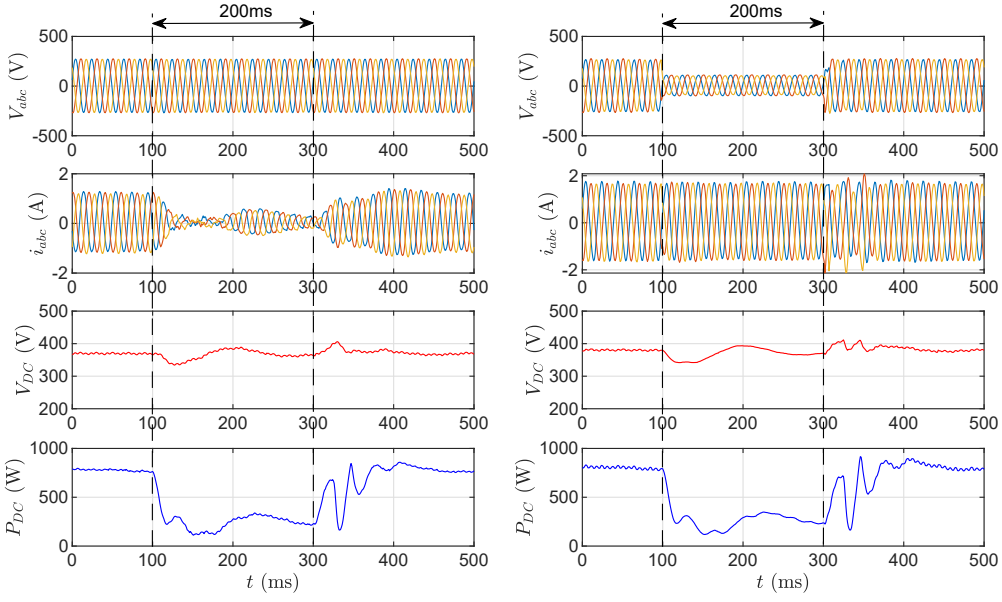

(a) VSC1 (b) VSC2

Fig. 4. Case 1: Experimental waveforms with FRT control at P_{sref2} = 80%, Q_{sref2} = 0% before, while, and after a three-phase voltage sag with a depth of 60% and a duration time of 200 ms occurred in Grid 2

as shown in the first plot of Fig. 4(a). However, the controller of the VSC-HVDC system will control in order to maintain power supply of the system. In this case, the DC-link voltages of both VSC1 and VSC2 are almost flat, as clearly shown in the third plot of Fig. 4(a) and Fig. 4(b), due to the converter system VSC1. The magnitude of three-phase currents of VSC1 is decreased in the period between 100 ms and 300 ms, as shown in the second plot of Fig. 4(a), while the magnitude of three-phase currents of VSC2 is still stable, as shown in the second plot of Fig. 4(b). During the entire voltage sag period from 100 ms to 300 ms, the DC power of both VSC1 and VSC2, as shown in the fourth plot of Fig. 4(a) and Fig. 4(b), is reduced. After the voltage sag ends, a transient state appears in the waveforms for a short time and then the system's parameters comeback to the steady state, same as the state before the voltage sag. This means the VSC-HVDC transmission system is still normally operated to transmit an active and reactive power (P_{sref2} = 800 W, Q_{sref2} = 0 kVAR) from Grid 1 to Grid 2 after the three-phase voltage sag with a depth of 60% and a time duration of 200 ms occurred in Grid 2.

In the state-space representation, after applying the Park transformation into the dq-axis, Fig. 5 shows the dq-components of the voltage and current of the two converter systems which were also recorded when we carried out Case 1. Fig. 5(a) shows clearly that the d-component of the AC voltage at VSC1 (V_{sd1}) is still constant but the d-component of the AC voltage at VSC2 (V_{sd2}) is dramatically reduced during the period of the three-phase voltage sag, that occurred in Grid 2. Before, while and after the fault, three-phase voltages of VSC1 and VSC2 are perfectly balanced; therefore, their q-components (V_{sq1}, V_{sq2}) equal zero as shown in Fig. 5(a). Besides, the dq-components of the AC current at both VSC1 and VSC2 are shown in Fig. 5(b). As Fig. 5(b) shown, the d-component of the AC current at VSC1 (i_{d1}) is dramatically reduced during the period of the voltage sag but the d-component of the AC current at VSC2 (i_{d2}) is almost constant. The q-components (i_{q1}, i_{q2}) are shown in Fig. 5(b). The experimental results in Fig. 5 also show that after the duration time of the three-phase voltage sag, the voltage and current of both VSC1 and VSC2 of the VSC-HVDC transmission system is normal therefore the VSC-HVDC system is not disconnected.

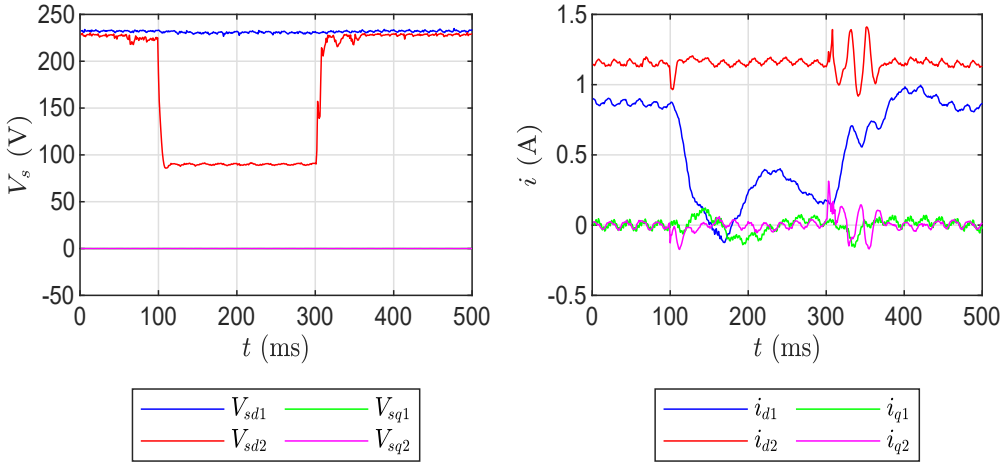

(a) Voltage (b) Current

Fig. 5. Case 1: The dq-components of the voltage and current of VSC1 and VSC2

Case 2: Two-phase voltage sag

In this case, a two-phase voltage sag is created by using the dynamic grid fault simulation in the experimental setup shown in Fig. 3. The voltage sag also occurs in Grid 2 with a remaining voltage of 60%, and a duration time of 200 ms. The entire experimental results of Case 2 are also recorded in a total time of 500 ms and are plotted in Fig. 6(a) and Fig. 6(b) for VSC1 and VSC2, respectively. In each figure, the first and second plots represent the three-phase voltage and current waveforms at the AC grid to which the VSC is connected, the third and fourth plots show the DC voltage and the DC power at the DC-link circuit of the VSC. As the first plot of Fig. 6(b) shown, the voltage magnitude of two phases (phase B and phase C) decreased to 60% of the nominal voltage and the phase A voltage magnitude still does not vary during the period of the voltage sag (from 100 ms to 300 ms). At VSC1, as shown on the first plot of Fig. 6(a), the voltage sag at Grid 2 has no effect on the three-phase voltage waveform of VSC1. This means the three-phase voltage waveform of VSC1 remained stable. Under the FRT requirement of the VSC-HVDC transmission system, the VSC2 controller will control to maintain the power transmission on the DC cable from Grid 1 to Grid 2, according to the active power reference $P_{sref2} = 80\%$ or $P_{sref2} = 800$ W. This is clearly shown on three plots of each figure which represent the three-phase current, DC-link voltage, and DC power of each converter system. From the experimental results of Case 2, we conclude that the VSC-HVDC transmission system will still maintain its operation after the two-phase voltage sag with a remaining voltage of 60% and a duration time of 200 ms occurred in Grid 2.

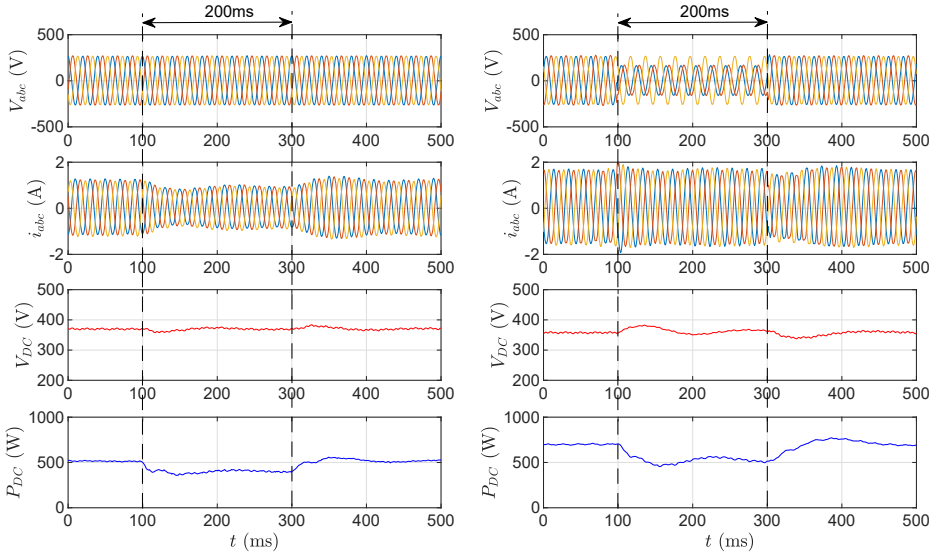

(a) VSC1 (b) VSC2

Fig. 6. Case 2: Experimental waveforms with FRT control at $P_{sref2} = 80\%$, $Q_{sref2} = 0\%$ before, while, and after a two-phase voltage sag with a depth of 60% and a duration time of 200 ms occurred in Grid 2

Applying the Park transformation into dq-axis, the dq-components of three-phase voltage and current of the two converter systems are recorded and plotted in Fig. 7(a) and Fig. 7(b).

The dq-components of the voltage of the two converter systems are shown in Fig. 7(a). In Fig. 7(a), the d-component of the voltage of VSC1 V_{sd1} (blue line) is almost flat but the d-component of the voltage of VSC2 V_{sd2} (red line) is reduced in the period from 100 ms to 300 ms. Before, while and after the fault, three-phase voltages of VSC1 and VSC2 are perfectly balanced; therefore, their q-components (green line and magenta line) equal zero ($V_{sq1} = V_{sq2} = 0$), as shown in Fig. 7(a). Besides, the dq-components of the current of the two converter systems are shown in Fig. 7(b). As we can see in Fig. 7(b), the q-components of the currents (i_{q1} and i_{q2}) almost equal zero due to its balance, but the d-components (i_{d1} and i_{d2}) are varied as the blue line and the red line show in Fig. 7(b). Moreover, these experimental results also show that after the voltage sag ends, the voltage and current of the two converters come back as the initial steady state. Therefore, the VSC-HVDC transmission system can ride-through a two-phase voltage sag with a remaining voltage of 60% and a duration time of 200 ms.

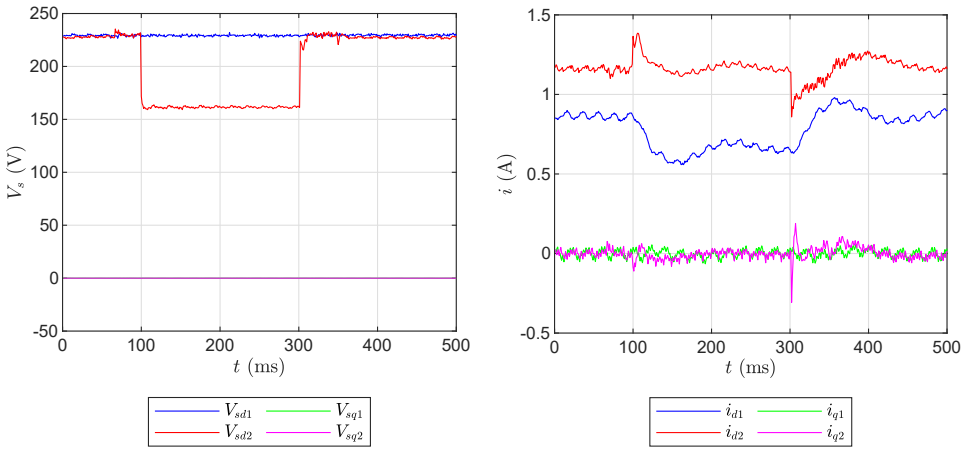

(a) Voltage (b) Current

Fig. 7. Case 2: The dq-components of the voltage and current of VSC1 and VSC2

Case 3: Single-phase voltage sag

In the third case study, a single-phase voltage sag with a depth of 60% and a duration time of 200 ms is generated by using the dynamic grid fault simulator in order to investigate the FRT capability of the VSC-HVDC transmission system of Smart Grid Laboratory. In the initial steady state, the converter system, VSC2, is also set up to transmit an active power of 80% power rating ($P_{\text{ref2}} = 80\%$ or $P_{\text{ref2}} = 800$ W) and a reactive power of 0% power rating ($Q_{\text{ref2}} = 0\%$ or $Q_{\text{ref2}} = 0$ kVAR) from Grid 1 to Grid 2. The single-phase voltage sag at Grid 2 starts at 100 ms and lasts for 200 ms, as shown in the first plot of Fig. 8(b). The voltage waveform in the first plot of Fig. 8(a) represents three-phase voltages of VSC1 which is still stable during the entire recording time. Under the FRT requirement of the VSC-HVDC transmission system, its controller will control to maintain the power transmission in the DC cable from Grid 1 to Grid 2, according to the active and reactive power reference ($P_{s\text{ref2}} = 80\%$ or $P_{s\text{ref2}} = 800$ W and $Q_{s\text{ref2}} = 0\%$ or $Q_{s\text{ref2}} = 0$ kvar). According to these experimental waveforms, we conclude that the VSC-HVDC transmission system will still stay connected after the single-phase voltage sag with a depth of

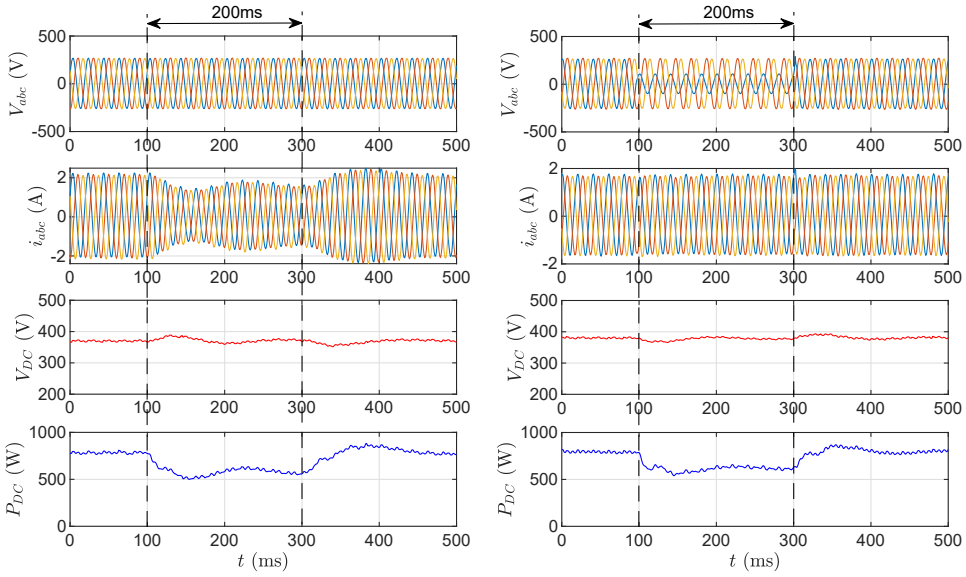

(a) VSC1 (b) VSC2

Fig. 8. Case 3: Experimental waveforms with FRT control at P_{sref2} = 80%, Q_{sref2} = 0% before, while, and after a single-phase voltage sag with a depth of 60% and a duration time of 200 ms occurred in Grid 2

60% and a duration time of 200 ms occurred in Grid 2. Moreover, the experimental parameters including V_{sd1}, V_{sq1}, V_{sd2}, V_{sq2}, i_{d1}, i_{q1}, i_{d2}, and i_{q2} represent the dq-components of the voltage and current at VSC1 as well as VSC2, and are recorded and plotted in Fig. 9(a) and Fig. 9(b) when we carry on with this case. These experimental parameters show that the VSC-HVDC can completely ride through the single-phase voltage sag.

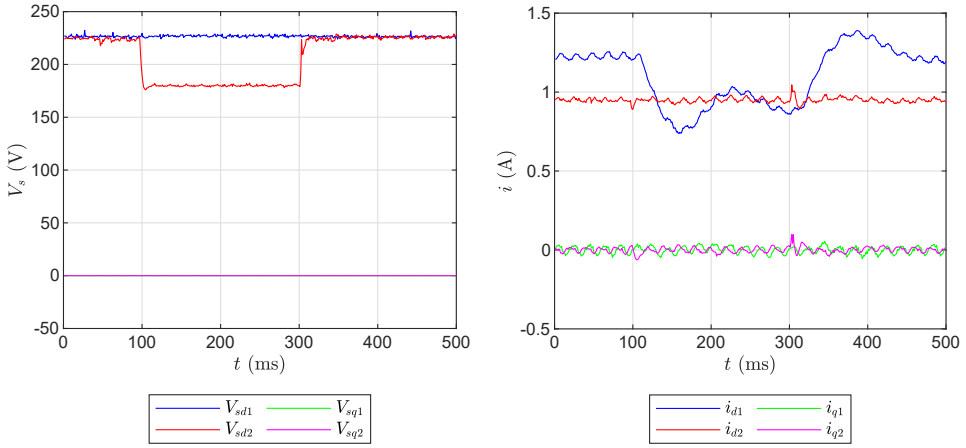

(a) Voltage (b) Current

Fig. 9. Case 3: The dq-components of the voltage and current of VSC1 and VSC2

According to the analysis of the experimental results mentioned above, the requirement is applied to evaluate the FRT capability of the VSC-HVDC transmission system. Hence, the d-components of the voltages at VSC2 in three case studies are plotted on the FRT profile, as shown in Fig. 10. As in the previous section, three voltage sag events of three case studies have a same depth of 60% and a same duration time of 200 ms. However, the three-phase voltage sag for Case 1, the two-phase voltage sag for Case 2, and the single-phase voltage sag for Case 3 are carried out. Therefore, the d-components of these voltage sag events after using the Park transformation will vary, as shown clearly in Fig. 10. From these experimental results, it can be seen that the VSC-HVDC transmission system can overcome three faults in order to stay connected.

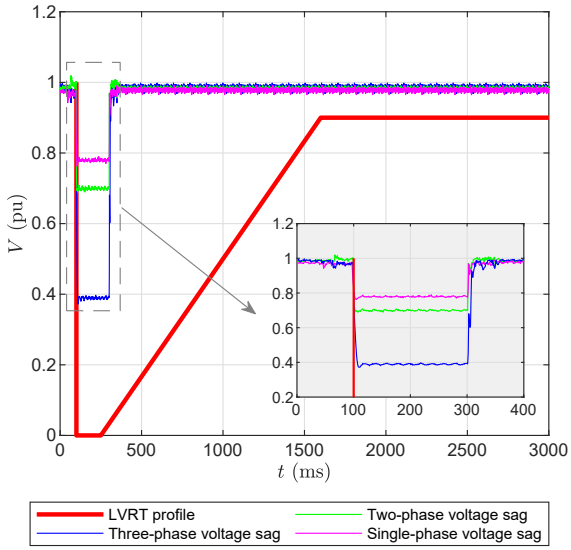

Fig. 10. The comparision between the experimental results and FRT requirement

4. Conclusions

A practical method has been developed in this research work for investigating the FRT capability of the VSC-HVDC transmission system in a laboratory environment. The effectiveness of this method is to show clearly the operation status of the VSC-HVDC in real time and all recorded data can also be used to compare with the FRT requirement. The symmetrical and asymmetrical voltage sag events are generated by using the dynamic grid fault simulator to verify the control performance of the converter systems. Three case studies including three-phase voltage sag, two-phase voltage sag, and single-phase voltage sag have been extensively carried out to record the voltage and current waveforms at the converter systems. The experimental results of each case study are compared with the FRT requirement of the VSC-HVDC system to evaluate its FRT capability. The experimental results show the FRT capability and its performance during a network fault and they are thoroughly addressed in this paper.

Future works will be undertaken on the following aspects: (*i*) New control methods of VSCs will be studied to update the hardware units of the experimental setup; (*ii*) The integration of the experimental module of a doubly-fed induction generator (DFIG) wind turbine using the VSC-HVDC system will be also investigated.

References

[1] Hingorani N., Gyugyi L., *Understanding FACTS: Concepts and Technology of Flexible AC Transmission Systems*, IEEE Press, Willey (2000).

[2] Zhang X.P., Rehtanz C., Pal B., *Flexible AC Transmission Systems: Modelling and Control*, Springer-Verlag (2006).

[3] Yazdani A., Iravani R., *Voltage-sourced converters in power systems: Modeling, Control, and Applications*, IEEE Press, Wiley (2010).

[4] Flourentzou N., Agelidis V.G., Demetriades G.D., *VSC-Based HVDC Power Transmission Systems: An Overview*, IEEE Transactions on Power Electronics, vol. 24, pp. 592–602 (2009).

[5] Sessa S.D., Chiarelli A., Benato R., *Availability Analysis of HVDC-VSC Systems: A Review*, Energies, vol. 12, no. 14, pp. 1–22 (2019), DOI: 10.3390/en12142703.

[6] Alassi A., Bañales S., Ellabban O., Adam G., MacIver C., *HVDC Transmission: Technology Review, Market Trends and Future Outlook*, Renewable and Sustainable Energy Reviews, vol. 112, pp. 530–554 (2019), DOI: 10.1016/j.rser.2019.04.062.

[7] Patil P.R., Bhole A.A., *A review on enhancing fault ride-through capability of distributed generation in a microgrid*, In Proceedings of 2017 Innovations in Power and Advanced Computing Technologies (i-PACT), April 21–22, Vellore, India (2017), DOI: 10.1109/IPACT.2017.8245189.

[8] Yaramasu V., Wu B., Sen P.C., Kouro S., Narimani M., *High-power wind energy conversion systems: State-of-the-art and emerging technologies*, Proceedings of the IEEE, vol. 103, pp. 740–788 (2015).

[9] Feltes C., Wrede H., Koch F.W., Erlich I., *Enhanced fault ride-through method for wind farms connected to the grid through VSC-based HVDC transmission*, IEEE Transactions on Power Systems, vol. 24, pp. 1537–1546 (2009).

[10] Sang Y., Yang B., Shu H., An N., Zeng F., Yu T., *Fault Ride-Through Capability Enhancement of Type-4 WECS in Offshore Wind Farm via Nonlinear Adaptive Control of VSC-HVDC*, Processes, vol. 7, no. 540 (2019), DOI: 10.3390/pr7080540.

[11] Vrionis T.D., Koutiva X.I., Vovos N.A., Giannakopoulos G.B., *Control of an HVDC Link Connecting a Wind Farm to the Grid for Fault Ride-Through Enhancement*, IEEE Transactions on Power Systems, vol. 22, no. 4, pp. 2039–2047 (2007).

[12] Ramtharan G., Arulampalam A., Ekanayake J.B., Hughes F., Jenkins N., *Fault ride through of fully rated converter wind turbines with AC and DC transmission systems*, IET Renewable Power Generation, vol. 3, iss. 4, pp. 426–438 (2009).

[13] Sun W., Torres-Olguina R.E., Anaya-Laraa O., *Investigation on Fault-ride through Methods for VSC-HVDC Connected Offshore Wind Farms*, Energy Procedia, vol. 94, pp. 29–36 (2016).

[14] Haleem N.M., Rajapakse A.D., Gole A.M., Fernando I.T., *Investigation of Fault Ride-Through Capability of Hybrid VSC-LCC Multi-Terminal HVDC Transmission Systems*, IEEE Transactions on Power Delivery, vol. 34, iss. 1, pp. 241–250 (2019).

[15] Li Y., Liu C., Tian X., Wang Z., *Study on fault ride-through control of islanded wind farm connected to VSC-HVDC grid based on the VSC converter AC-side bus forced short circuit*, The Journal of Engineering, vol. 2019, no. 16, pp. 3325–3328 (2019).

[16] Moawwad A., El Moursi M.S., Xiao W., *Advanced fault ride-through management scheme for VSC-HVDC connecting offshore wind farms*, IEEE Transactions on Power Systems, vol. 31, no. 6, pp. 4923–4934 (2016).

[17] Zhou Z., Chen Z., Wang X., Du D., Yang G., Wang Y., Hao L., *AC fault ride through control strategy on inverter side of hybrid HVDC transmission systems*, Journal of Modern Power Systems and Clean Energy, vol. 7, iss. 5, pp. 1129–1141 (2019).

[18] Feldman R., Farr E., Watson A.J., Clare J.C., Wheeler P.W., Trainer D.R., Crookes R.W., *DC fault ride-through capability and STATCOM operation of a HVDC hybrid voltage source converter*, IET Generation, Transmission and Distribution, vol. 8, iss. 1, pp. 114–120 (2014).

[19] Oguma K., Akagi H., *Low-Voltage-Ride-Through Performance of an HVDC Transmission System Using Two Modular Multilevel Double-Star Chopper-Cells Converters*, Electrical Engineering in Japan, vol. 200, pp. 33–44 (2017), DOI: 0.1109/TPEL.2016.2615048.

[20] Yang B., Sang Y.Y., Shi K., Yao W., Jiang L., Yu T., *Design and real-time implementation of perturbation observer based sliding-mode control for VSC-HVDC systems*, Control Engineering Practice, vol. 56, pp. 13–26 (2016).

[21] Yang B., Jiang L., Yu T., Shua H.C., Zhang C.K., Yao W., Wu Q.H., *Passive control design for multi-terminal VSC-HVDC systems via energy shaping*, International Journal of Electrical Power and Energy Systems, vol. 98, pp. 496–508 (2018).

[22] Dumnic B., Popadic B., Milicevic D., Vukajlovic N., Delimar M., *Control Strategy for a Grid Connected Converter in Active Unbalanced Distribution Systems*, Energies, vol. 12, no. 7 (2019), DOI: 10.3390/en12071362.

[23] Latorre H.F., Ghandhari M., Soder L., *Active and Reactive Power Control of VSC-HVDC*, Electrical Power System Research, vol. 78, pp. 1756–1763 (2008).

[24] Li C., Li Y., Guo J., He P., *Research on emergency DC power support coordinated control for hybrid multi-infeed HVDC system*, Archives of Electrical Engineering, vol. 69, no. 1, pp. 5–21 (2020).

[25] Yang B., Yu T., Zhang X., Huang L., Shu H., Jiang L., *Interactive teaching-learning optimizer for parameter tuning of VSC-HVDC systems with offshore wind farm integration*, IET Generation, Transmission and Distribution, vol. 12, no. 3, pp. 678–687 (2018).